Measurement of the transverse spin correlations in the decay $Z \to \tau^+\tau^-$

R. Barate, D. Buskulic, D. Decamp, P. Ghez, C. Goy, J P. Lees, A. Lucotte, M N. Minard, J y. Nief, B. Pietrzyk, et al.

HAL Id: in2p3-00005697

http://hal.in2p3.fr/in2p3-00005697

Submitted on 25 Jul 2000

Measurement of the transverse spin correlations in the decay $Z \to \tau^+\tau^-$

The ALEPH Collaboration[*]

Abstract

For τ leptons produced in $e^+e^- \to \tau^+\tau^-$ interactions there are, in addition to the longitudinal spin correlations, two independent transverse spin correlations associated with the transverse (within the production plane) and normal (to the production plane) polarization components. A measurement of the transverse-transverse and transverse-normal τ spin correlations in the decay $Z \to \tau^+\tau^-$, C_{TT} and C_{TN}, is presented based on the aplanarity angle of the decay products of both τ leptons. Using 80 pb^{-1} of data collected by ALEPH on the peak of the Z resonance, the results are $C_{\mathrm{TT}} = 1.06 \pm 0.13(stat) \pm 0.05(syst)$, and $C_{\mathrm{TN}} = 0.08 \pm 0.13(stat) \pm 0.04(syst)$. These values are in agreement with the Standard Model predictions, $C_{\mathrm{TT}} = 0.99$ and $C_{\mathrm{TN}} = -0.01$.

---

[*]See the following pages for the list of authors.

The ALEPH Collaboration

R. Barate, D. Buskulic, D. Decamp, P. Ghez, C. Goy, J.-P. Lees, A. Lucotte, M.-N. Minard, J.-Y. Nief, B. Pietrzyk

Laboratoire de Physique des Particules (LAPP), IN²P³-CNRS, 74019 Annecy-le-Vieux Cedex, France

M.P. Casado, M. Chmeissani, P. Comas, J.M. Crespo, M. Delfino, E. Fernandez, M. Fernandez-Bosman, Ll. Garrido,[15] A. Juste, M. Martinez, R. Miquel, Ll.M. Mir, S. Orteu, C. Padilla, I.C. Park, A. Pascual, J.A. Perlas, I. Riu, F. Sanchez, F. Teubert

Institut de Física d'Altes Energies, Universitat Autònoma de Barcelona, 08193 Bellaterra (Barcelona), Spain[7]

A. Colaleo, D. Creanza, M. de Palma, G. Gelao, G. Iaselli, G. Maggi, M. Maggi, N. Marinelli, S. Nuzzo, A. Ranieri, G. Raso, F. Ruggieri, G. Selvaggi, L. Silvestris, P. Tempesta, A. Tricomi,[3] G. Zito

Dipartimento di Fisica, INFN Sezione di Bari, 70126 Bari, Italy

X. Huang, J. Lin, Q. Ouyang, T. Wang, Y. Xie, R. Xu, S. Xue, J. Zhang, L. Zhang, W. Zhao

Institute of High-Energy Physics, Academia Sinica, Beijing, The People's Republic of China[8]

D. Abbaneo, R. Alemany, U. Becker, A.O. Bazarko,[20] P. Bright-Thomas, M. Cattaneo, F. Cerutti, G. Dissertori, H. Drevermann, R.W. Forty, M. Frank, R. Hagelberg, J.B. Hansen, J. Harvey, P. Janot, B. Jost, E. Kneringer, J. Knobloch, I. Lehraus, G. Lutters, P. Mato, A. Minten, L. Moneta, A. Pacheco, J.-F. Pusztaszeri,[23] F. Ranjard, G. Rizzo, L. Rolandi, D. Rousseau, D. Schlatter, M. Schmitt, O. Schneider, W. Tejessy, I.R. Tomalin, H. Wachsmuth, A. Wagner[24]

European Laboratory for Particle Physics (CERN), 1211 Geneva 23, Switzerland

Z. Ajaltouni, A. Barrès, C. Boyer, A. Falvard, C. Ferdi, P. Gay, C. Guicheney, P. Henrard, J. Jousset, B. Michel, S. Monteil, J-C. Montret, D. Pallin, P. Perret, F. Podlyski, J. Proriol, P. Rosnet, J.-M. Rossignol

Laboratoire de Physique Corpusculaire, Université Blaise Pascal, IN²P³-CNRS, Clermont-Ferrand, 63177 Aubière, France

T. Fearnley, J.D. Hansen, J.R. Hansen, P.H. Hansen, B.S. Nilsson, B. Rensch, A. Wäänänen

Niels Bohr Institute, 2100 Copenhagen, Denmark[9]

G. Daskalakis, A. Kyriakis, C. Markou, E. Simopoulou, I. Siotis, A. Vayaki

Nuclear Research Center Demokritos (NRCD), Athens, Greece

A. Blondel, G. Bonneaud, J.C. Brient, P. Bourdon, A. Rougé, M. Rumpf, A. Valassi,[6] M. Verderi, H. Videau

Laboratoire de Physique Nucléaire et des Hautes Energies, Ecole Polytechnique, IN²P³-CNRS, 91128 Palaiseau Cedex, France

D.J. Candlin, M.I. Parsons

Department of Physics, University of Edinburgh, Edinburgh EH9 3JZ, United Kingdom[10]

E. Focardi, G. Parrini, K. Zachariadou

Dipartimento di Fisica, Università di Firenze, INFN Sezione di Firenze, 50125 Firenze, Italy

M. Corden, C. Georgiopoulos, D.E. Jaffe

Supercomputer Computations Research Institute, Florida State University, Tallahassee, FL 32306-4052, USA [13,14]

A. Antonelli, G. Bencivenni, G. Bologna,[4] F. Bossi, P. Campana, G. Capon, D. Casper, V. Chiarella, G. Felici, P. Laurelli, G. Mannocchi,[5] F. Murtas, G.P. Murtas, L. Passalacqua, M. Pepe-Altarelli

Laboratori Nazionali dell'INFN (LNF-INFN), 00044 Frascati, Italy

L. Curtis, S.J. Dorris, A.W. Halley, I.G. Knowles, J.G. Lynch, V. O'Shea, C. Raine, J.M. Scarr, K. Smith, P. Teixeira-Dias, A.S. Thompson, E. Thomson, F. Thomson, R.M. Turnbull

Department of Physics and Astronomy, University of Glasgow, Glasgow G12 8QQ, United Kingdom[10]

C. Geweniger, G. Graefe, P. Hanke, G. Hansper, V. Hepp, E.E. Kluge, A. Putzer, M. Schmidt, J. Sommer, K. Tittel, S. Werner, M. Wunsch

Institut für Hochenergiephysik, Universität Heidelberg, 69120 Heidelberg, Fed. Rep. of Germany[16]

R. Beuselinck, D.M. Binnie, W. Cameron, P.J. Dornan, M. Girone, S. Goodsir, E.B. Martin, A. Moutoussi, J. Nash, J.K. Sedgbeer, P. Spagnolo, A.M. Stacey, M.D. Williams

Department of Physics, Imperial College, London SW7 2BZ, United Kingdom[10]

V.M. Ghete, P. Girtler, D. Kuhn, G. Rudolph

Institut für Experimentalphysik, Universität Innsbruck, 6020 Innsbruck, Austria[18]

A.P. Betteridge, C.K. Bowdery, P. Colrain, G. Crawford, A.J. Finch, F. Foster, G. Hughes, R.W. Jones, T. Sloan, M.I. Williams

Department of Physics, University of Lancaster, Lancaster LA1 4YB, United Kingdom[10]

A. Galla, I. Giehl, A.M. Greene, C. Hoffmann, K. Jakobs, K. Kleinknecht, G. Quast, B. Renk, E. Rohne, H.-G. Sander, P. van Gemmeren, C. Zeitnitz

Institut für Physik, Universität Mainz, 55099 Mainz, Fed. Rep. of Germany[16]

J.J. Aubert, C. Benchouk, A. Bonissent, G. Bujosa, D. Calvet, J. Carr, P. Coyle, C. Diaconu, F. Etienne, N. Konstantinidis, O. Leroy, F. Motsch, P. Payre, M. Talby, A. Sadouki, M. Thulasidas, K. Trabelsi

Centre de Physique des Particules, Faculté des Sciences de Luminy, IN^{2}P^3-CNRS, 13288 Marseille, France

M. Aleppo, F. Ragusa[2]

Dipartimento di Fisica, Università di Milano e INFN Sezione di Milano, 20133 Milano, Italy

R. Berlich, W. Blum, V. Büscher, H. Dietl, G. Ganis, C. Gotzhein, H. Kroha, G. Lütjens, G. Lutz, W. Männer, H.-G. Moser, R. Richter, A. Rosado-Schlosser, S. Schael, R. Settles, H. Seywerd, R. St. Denis, H. Stenzel, W. Wiedenmann, G. Wolf

Max-Planck-Institut für Physik, Werner-Heisenberg-Institut, 80805 München, Fed. Rep. of Germany[16]

J. Boucrot, O. Callot,[2] S. Chen, Y. Choi,[21] A. Cordier, M. Davier, L. Duflot, J.-F. Grivaz, Ph. Heusse, A. Höcker, A. Jacholkowska, M. Jacquet, D.W. Kim,[12] F. Le Diberder, J. Lefrançois, A.-M. Lutz, I. Nikolic, M.-H. Schune, S. Simion, E. Tournefier, J.-J. Veillet, I. Videau, D. Zerwas

Laboratoire de l'Accélérateur Linéaire, Université de Paris-Sud, IN^{2}P^3-CNRS, 91405 Orsay Cedex, France

P. Azzurri, G. Bagliesi, G. Batignani, S. Bettarini, C. Bozzi, G. Calderini, M. Carpinelli, M.A. Ciocci, V. Ciulli, R. Dell'Orso, R. Fantechi, I. Ferrante, L. Foà,[1] F. Forti, A. Giassi, M.A. Giorgi, A. Gregorio, F. Ligabue, A. Lusiani, P.S. Marrocchesi, A. Messineo, F. Palla, G. Sanguinetti, A. Sciabà, J. Steinberger, R. Tenchini, G. Tonelli,[19] C. Vannini, A. Venturi, P.G. Verdini

Dipartimento di Fisica dell'Università, INFN Sezione di Pisa, e Scuola Normale Superiore, 56010 Pisa, Italy

G.A. Blair, L.M. Bryant, J.T. Chambers, Y. Gao, M.G. Green, T. Medcalf, P. Perrodo, J.A. Strong, J.H. von Wimmersperg-Toeller

Department of Physics, Royal Holloway & Bedford New College, University of London, Surrey TW20 OEX, United Kingdom[10]

D.R. Botterill, R.W. Clifft, T.R. Edgecock, S. Haywood, P. Maley, P.R. Norton, J.C. Thompson, A.E. Wright

Particle Physics Dept., Rutherford Appleton Laboratory, Chilton, Didcot, Oxon OX11 OQX, United Kingdom[10]

B. Bloch-Devaux, P. Colas, S. Emery, W. Kozanecki, E. Lançon, M.C. Lemaire, E. Locci, P. Perez, J. Rander, J.-F. Renardy, A. Roussarie, J.-P. Schuller, J. Schwindling, A. Trabelsi, B. Vallage

CEA, DAPNIA/Service de Physique des Particules, CE-Saclay, 91191 Gif-sur-Yvette Cedex, France[17]

S.N. Black, J.H. Dann, R.P. Johnson, H.Y. Kim, A.M. Litke, M.A. McNeil, G. Taylor

Institute for Particle Physics, University of California at Santa Cruz, Santa Cruz, CA 95064, USA[22]

C.N. Booth, R. Boswell, C.A.J. Brew, S. Cartwright, F. Combley, M.S. Kelly, M. Lehto, W.M. Newton, J. Reeve, L.F. Thompson

Department of Physics, University of Sheffield, Sheffield S3 7RH, United Kingdom[10]

A. Böhrer, S. Brandt, G. Cowan, C. Grupen, P. Saraiva, L. Smolik, F. Stephan

Fachbereich Physik, Universität Siegen, 57068 Siegen, Fed. Rep. of Germany[16]

M. Apollonio, L. Bosisio, R. Della Marina, G. Giannini, B. Gobbo, G. Musolino

Dipartimento di Fisica, Università di Trieste e INFN Sezione di Trieste, 34127 Trieste, Italy

J. Rothberg, S. Wasserbaech

Experimental Elementary Particle Physics, University of Washington, WA 98195 Seattle, U.S.A.

S.R. Armstrong, E. Charles, P. Elmer, D.P.S. Ferguson, S. González, T.C. Greening, O.J. Hayes, H. Hu, S. Jin, P.A. McNamara III, J.M. Nachtman, J. Nielsen, W. Orejudos, Y.B. Pan, Y. Saadi, I.J. Scott, J. Walsh, Sau Lan Wu, X. Wu, J.M. Yamartino, G. Zobernig

Department of Physics, University of Wisconsin, Madison, WI 53706, USA[11]

1   Introduction

The longitudinal polarization of the τ produced in the reaction $e^+e^- \to \tau^+\tau^-$ at the Z resonance has been widely studied by all LEP experiments [1–4]. As a result, the Zee and $Z\tau\tau$ couplings have been precisely measured and as a consequence the weak mixing angle $\sin^2\theta_W^{\text{eff}}$ is obtained. In addition to the longitudinal spin polarization of each τ lepton, three independent spin-spin correlations can be measured. These are the longitudinal spin correlation and two transverse spin correlations associated with the transverse (within the production plane) and normal (to the production plane) polarization components: the transverse-transverse spin correlation C_{TT} and the transverse-normal spin correlation C_{TN} [5]. The presence of transverse spin correlations is a consequence of the conservation of angular momentum but their size depends on the coupling constants which are predicted by the Standard Model.

In this paper the transverse spin correlations are investigated by analyzing the angular distribution of the decay products of the τ pair. This is in contrast to the measurement of the longitudinal τ polarization which is mainly based on the energy spectra of the decay products. The following decay modes are used in this analysis: $\tau \to e\nu\nu$, $\mu\nu\nu$, $\pi\nu$, and $\rho\nu$.

The precision of the vector and axial vector coupling constants of the τ lepton, v_τ and a_τ, and of $\sin^2\theta_W^{\text{eff}}$ which can be obtained from this measurement is not competitive with that obtained from the standard observables of τ pair production: the total cross section, the forward-backward asymmetry, and the longitudinal polarization. However, it is certainly desirable to carry out a general test of the coupling structure of the theory [6]. As a part of this programme limits on the the weak dipole moment have already been obtained [7]. The correlations C_{TT} and C_{TN} yield information which is independent of any anomalous dipole moment [6]. Moreover, C_{TT} is proportional to $|a_\tau|^2 - |v_\tau|^2$ and therefore its sign enables the ambiguity between a_τ and v_τ in a purely weak process to be resolved, whereas so far it has only been resolved from γ-Z interference. The transverse-normal spin correlation C_{TN} is both a parity-odd and time-reversal-odd observable that vanishes for Z exchange at tree level. In the Standard Model it receives small contributions from γ-Z interference and from the absorptive part of the electroweak amplitudes generated at one-loop level [8]. A value sizably different from zero could indicate CP violation from a source other than a τ dipole moment.

The paper is organized as follows. Section 2 describes the theoretical framework to compute the cross-section, including the transverse spin correlations, as a function of three angles. Section 3 describes the data analysis. Systematic errors are treated in section 4. In section 5 the measurements of the transverse spin correlations are presented. Finally, section 6 contains the summary.

2 Theory

2.1 Standard Model

The Standard Model cross-section for the process $e^+e^- \to \tau^+\tau^-$ around the Z peak, which includes the dependence on the τ spins but neglects the γ exchange contribution, is given by [5]

$$
\begin{aligned}
\frac{d\sigma(\hat{s}_{\tau-}, \hat{s}_{\tau+})}{d\Omega_{\tau-}} = \; & \frac{1}{4q^2}|P(q^2)|^2 \{ C_0(1 + \cos^2\theta) + 2C_1 \cos\theta \\
& - D_0(s^L_{\tau-} - s^L_{\tau+})(1 + \cos^2\theta) - D_1(s^L_{\tau-} - s^L_{\tau+})2\cos\theta \\
& - C_0 s^L_{\tau-} s^L_{\tau+}(1 + \cos^2\theta) - C_1 s^L_{\tau-} s^L_{\tau+} 2\cos\theta \\
& + C_2(s^N_{\tau-} s^N_{\tau+} - s^T_{\tau-} s^T_{\tau+})\sin^2\theta + D_2(s^N_{\tau-} s^T_{\tau+} + s^T_{\tau-} s^N_{\tau+})\sin^2\theta \}
\end{aligned}
$$

where

$$
\begin{aligned}
P(q^2) &= \frac{\alpha}{4s^2_W(1 - s^2_W)} \; \frac{q^2}{q^2 - M_Z^2 + iq^2\Gamma_Z/M_Z} \\
C_0 &= (|v_e|^2 + |a_e|^2)(|v_\tau|^2 + |a_\tau|^2) \\
C_1 &= 4\mathrm{Re}(v_e a_e^*)\mathrm{Re}(v_\tau a_\tau^*) \\
C_2 &= (|v_e|^2 + |a_e|^2)(|a_\tau|^2 - |v_\tau|^2) \\
D_0 &= 2\mathrm{Re}(v_\tau a_\tau^*)(|v_e|^2 + |a_e|^2) \\
D_1 &= 2\mathrm{Re}(v_e a_e^*)(|v_\tau|^2 + |a_\tau|^2) \\
D_2 &= -2\mathrm{Im}(v_\tau a_\tau^*)(|v_e|^2 + |a_e|^2).
\end{aligned}
\tag{1}
$$

In these expressions v_f and a_f are the effective (complex) vector and axial vector Zff couplings, α is the fine-structure constant and $s^2_W(= \sin^2\theta^{\mathrm{eff}}_W)$ is the weak mixing parameter, $s^i_{\tau\pm}$ are the $\tau^\pm$ spin components,[1] q is the centre of mass energy, and M_Z (Γ_Z) is the mass (width) of the Z boson.

The coefficients C_2 and D_2 carry all the information about the transverse-transverse $(s^N_{\tau-} s^N_{\tau+} - s^T_{\tau-} s^T_{\tau+})$ and the transverse-normal $(s^N_{\tau-} s^T_{\tau+} + s^T_{\tau-} s^N_{\tau+})$ spin correlations. The measured spin correlations are defined by $C_{\mathrm{TT}} = C_2/C_0$ and $C_{\mathrm{TN}} = D_2/C_0$. At $\sqrt{s} = M_Z$, if $\gamma\text{-}Z$ interference is included, C_{TT} is essentially unchanged, whereas the term $(8s^2_W(1 - s^2_W)\mathrm{Re}(v_e a_\tau^*)\Gamma_Z)/(C_0 M_Z)$ has to be added to C_{TN}. For $\sin^2\theta_W = 0.23$ the Standard Model predicts $C_{\mathrm{TT}} = 0.99$ and $C_{\mathrm{TN}} = -0.01$ [5, 8].

In the analysis presented here only events at the Z peak are analyzed. The $\gamma\text{-}Z$ interference omitted in Eq. (1) plays a role for events with initial state radiation (ISR). This effect is taken into account in the theoretical expression used to fit the data.

---

[1]i=L designates the longitudinal component, i=T the transverse component within the production plane, and i=N is the transverse component normal to the production plane.
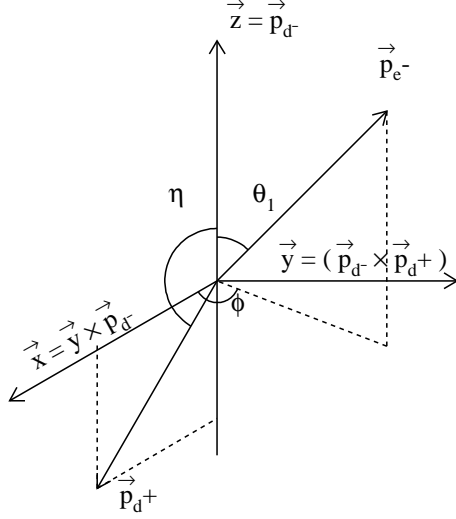
Figure 1: Coordinate system in the lab frame, $p_{d\pm}$ are the direction of the $\tau^{\pm}$ decay products, p_{e^-} is the direction of the incident e^-, p_{d^+} lies in the x-z plane.

The C_{TN} coefficient is given explicitly by

$$C_{\mathrm{TN}} \;\; = \;\; \frac{D_2}{C_0} = -2\frac{\mathrm{Im}(v_\tau a_\tau^*)}{|v_\tau|^2 + |a_\tau|^2} = -2\frac{|v_\tau||a_\tau|}{|v_\tau|^2 + |a_\tau|^2}\sin(\Phi_{v_\tau} - \Phi_{a_\tau}), \qquad (2)$$

where $v_\tau = |v_\tau|e^{i\Phi_{v_\tau}}$ and $a_\tau = |a_\tau|e^{i\Phi_{a_\tau}}$, while the longitudinal τ polarization $P_\tau = -D_0/C_0$ can be expressed in the same formalism as

$$P_\tau \;\; = \;\; -\frac{D_0}{C_0} = -2\frac{\mathrm{Re}(v_\tau a_\tau^*)}{|v_\tau|^2 + |a_\tau|^2} = -2\frac{|v_\tau||a_\tau|}{|v_\tau|^2 + |a_\tau|^2}\cos(\Phi_{v_\tau} - \Phi_{a_\tau}). \qquad (3)$$

The phase difference $\Phi_{v_\tau} - \Phi_{a_\tau}$ can be obtained using both measurements:

$$\tan(\Phi_{v_\tau} - \Phi_{a_\tau}) \;\; = \;\; \frac{C_{\mathrm{TN}}}{P_\tau}. \qquad (4)$$

2.2   Observables

As in the well known longitudinal polarization studies, the τ spin vectors are not directly measurable, but the τ decay products can be used as spin analyzers. The $\tau^+\tau^-$ spin correlations give rise to angular correlations of the decay products [5]. The distribution of the sequential process $e^+e^- \to \tau^+\tau^- \to X_i^+ X_j^- + ...$ can be written as a function of the polar angle of the negatively charged particle θ_1, the acollinearity η and aplanarity ϕ angles of the decay products (Fig. 1) [9]:

$$\frac{d^3\sigma^{ij}}{d\epsilon\, d\cos\theta_1\, d\phi} = \frac{|P(q^2)|^2}{4q^2}\{F_0^{ij}(\epsilon)(1 + \cos^2\theta_1) + F_1^{ij}(\epsilon)2\cos\theta_1 + F_2^{ij}(\epsilon,\phi)\sin^2\theta_1\}, \quad (5)$$

3

where i, j specify the τ decay channels, $\epsilon = \pi - \eta$, and

$$
\begin{aligned}
F_n^{ij}(\epsilon) &= C_n Q_1^{ij}(\epsilon) + D_n Q_2^{ij}(\epsilon), \quad n = 0, 1 \\
F_2^{ij}(\epsilon, \phi) &= \{C_2 \cos 2\phi + D_2 \sin 2\phi\} Q_3^{ij}(\epsilon).
\end{aligned}
\tag{6}
$$

The $Q_n^{ij}(\epsilon)$ functions are computed numerically using the TAUOLA Monte Carlo [10] describing the τ decay [9]. In this way, the mass of the τ decay products, vertex corrections, and photon radiation are included automatically in the final angular distributions.

Since the $\tau^+ \tau^-$ selection efficiency does not distinguish between the decay channels $\tau \to \pi \nu$ and $\tau \to K \nu$, the $Q_n^{ij}(\epsilon)$ functions are redefined as follows in order to take into account the π, K mass difference

$$
\begin{aligned}
Q_n^{i\pi}(\epsilon) &\to W_\pi Q_n^{i\pi}(\epsilon) + W_K Q_n^{iK}(\epsilon), \; i \neq \pi, K \\
Q_n^{\pi\pi}(\epsilon) &\to W_\pi W_\pi Q_n^{\pi\pi}(\epsilon) + W_K W_K Q_n^{KK}(\epsilon) + 2 W_\pi W_K Q_n^{\pi K}(\epsilon),
\end{aligned}
\tag{7}
$$

with $n = 1, 2, 3$, $W_\pi = B_{\tau \to \pi \nu} / [B_{\tau \to \pi \nu} + B_{\tau \to K \nu}]$, and $W_K = 1 - W_\pi$.

2.3 Fitting procedure

The correlations C_{TT} and C_{TN} are determined by a maximum likelihood fit of the cross-section Eq. (5) to the data, taking the experimental efficiencies and the initial state radiation correction into account. The correlations are obtained from the coefficients of the two terms depending on the aplanarity angle ϕ in Eq. (6). The following expression is maximized:

$$
\mathcal{L} = \sum_{ij} \sum_{n=1}^{N_{events}^{ij}} \ln \left(\sum_{kl} M_i^k M_j^l \frac{d^3 \Gamma_{kl}(q^2, \epsilon, \theta_1, \phi; C_{\mathrm{TT}}, C_{\mathrm{TN}})}{d\epsilon \, d\cos\theta_1 \, d\phi} \right),
\tag{8}
$$

where ij and kl describe the reconstructed and true $\tau^+ \tau^-$ decay channels, respectively, M_i^k is a matrix describing the probability that a channel k is reconstructed as channel i, N_{events}^{ij} is the number of selected events belonging to the class ij, and $d^3 \Gamma_{kl}/(d\epsilon \, d\cos\theta_1 \, d\phi)$ is the cross-section Eq. (5) corrected for the effect of the experimental efficiencies and the initial state radiation. The $Q_n^{ij}(\epsilon)$ functions have been computed by weighting TAUOLA Monte Carlo [10] events with the momentum dependence of the channel reconstruction efficiency obtained from the full detector simulation. This technique takes into account the different dependence of the three $Q_n^{ij}(\epsilon)(n = 1, 2, 3)$ functions on the momentum. On the other hand, the momentum is a variable which is not used in the fit. Therefore a check of the validity of the correction can be made by comparing the momentum and acollinearity distributions of data and Monte Carlo. The agreement is good over the full momentum range. The $Q_n^{ij}(\epsilon)$ functions for $\tau\tau$ background arising from the misidentification of the ρ and $\pi^\pm \pi^0 \pi^0$ final states are computed independently to take into account the different momentum

4

distributions.

Initial state radiation along the beam axis boosts the centre of mass reference system and therefore causes the initial electron beam and the two τ decay products to be coplanar ($\phi \to 0$ or π). The ISR distortion can be corrected due to the fact that the bulk of this effect has a kinematic origin [11]. Therefore the functions $Q_n^{ij}(\epsilon)$ computed at the Z centre of mass energy can be used at other energies by scaling the angle ϵ. As shown in [5] the $Q_n^{ij}(\epsilon)$'s are effectively functions of $\gamma\epsilon = \sqrt{s}/(2m_\tau)\epsilon$. If x is the fraction of the beam energy carried by the initial state photon and ϵ' is the angle which measures the acollinearity of an ISR event, the equivalent angle is given by

$$\epsilon'' = \epsilon'\sqrt{1-x}. \tag{9}$$

This approximation is valid for $\gamma^{-1} \ll 1$. γ^{-1} is smaller than 5% for values of the radiation parameter x smaller than 0.2 which is the limit used in the integration. The angular distribution is redefined as follows:

$$\frac{d^3\Gamma_{kl}}{d\epsilon\, d\cos\theta_1\, d\phi} = \int_0^{0.2} dx H(x) \frac{d^3\Gamma'_{kl}(M_Z^2(1-x), \epsilon'', \theta_1', \phi')}{d\epsilon''\, d\cos\theta_1'\, d\phi'} \frac{\partial(\epsilon', \theta_1', \phi')}{\partial(\epsilon, \theta_1, \phi)} \frac{\partial\epsilon''}{\partial\epsilon'}, \tag{10}$$

where the next to leading order ISR function $H(x)$ is described in [12] and the Jacobian $\partial(\epsilon', \theta_1', \phi')/\partial(\epsilon, \theta_1, \phi)$ takes into account the change in the three angles $(\epsilon, \theta_1, \phi)$ due to the boost. The $\gamma-Z$ interference terms appearing in $d^3\Gamma'_{kl}(M_Z^2(1-x))/(d\epsilon''\, d\cos\theta_1'\, d\phi')$ are fixed to the Standard Model values.

3   Data analysis

The data analyzed were recorded from 1992 to 1994 and represent an integrated luminosity of 80 pb^{-1}, all taken at the peak of the Z resonance, corresponding to about 120000 τ pairs.

3.1   ALEPH detector

The ALEPH detector is described in detail elsewhere [13, 14]. The main components to measure the energy and the momenta are the electromagnetic calorimeter (ECAL) and the tracking devices, namely the vertex detector (VDET), the inner tracking chamber (ITC) and the time projection chamber (TPC). The lepton identification relies on the dE/dx measurement in the TPC, on the ECAL, on the hadronic calorimeter (HCAL) and on the muon chambers.

3.2 $\tau^+\tau^-$ event selection and decay mode identification

The principal characteristics of the $\tau^+\tau^-$ events in e^+e^- annihilation are low multiplicity, back-to-back topology and missing energy. Each event is divided into

two hemispheres by a plane perpendicular to the thrust axis. The event is selected when there are less than eight charged tracks. Each hemisphere is required to have at least one good charged track. A good charged track is defined to have at least four reconstructed space points in the TPC, to extrapolate well to the interaction point, i.e. within ±2 cm transversally and ±10 cm along the beams. The $\tau^+\tau^-$ event selection consists of the identification of hemispheric τ decay channels plus several cuts that increase the purity of the sample.

The τ decay channels are classified in one of the following categories: $e^\pm, \mu^\pm, \pi^\pm(K^\pm), \rho^\pm$. Other τ decay channels are not selected because their sensitivity to transverse spin correlations is small [5]. The leading-momentum track in each hemisphere is identified as $e^\pm, \mu^\pm$, or $\pi^\pm(K^\pm)$ using the method described in [15], while π^0's are identified as described in [16]. A ρ particle is identified when the invariant mass of a π^0-$\pi^\pm$ pair falls inside the interval (0.44, 1.1) GeV/c^2. In addition, it is required that no identified objects, other than those mentioned, be present in either of the hemispheres. The final state identification in both hemispheres ensures that the contamination from non-τ pair events is small.

The background arises from $e^+e^- \rightarrow e^+e^-$, $e^+e^- \rightarrow \mu^+\mu^-$ and from $\tau^+\tau^-$ events with misidentified decay channels, although some contribution from $q\bar{q}$ and cosmic rays is still present in the selected sample. This background is reduced by means of additional cuts:

- $\tau^+\tau^-$ events leading to e^+e^- and $\mu^+\mu^-$ final states are simply not selected, since the sensitivity of those channels is in any case very small.

- $(E_1^{id} + E_2^{id}) < 80$ GeV when the event is identified as $\pi^\pm e^\mp$ or $\pi^\pm\mu^\mp$. E_i^{id} is the energy of the identified particle in the ith hemisphere. This reduces the Bhabha and dimuon contamination when either of the leptons is misidentified as a π.

- At least one of the good tracks must extrapolate to the interaction point within ±1 cm transversely and ±5 cm along the beam. This eliminates the possible cosmic-ray background.

- The fit is done within the range $0.5° < \epsilon < 9.0°$ for all the channels, except for $\rho^+\rho^-$ in which the upper limit is fixed to $4.0°$. These cuts reduce the $\gamma\gamma$, the Bhabha and the dimuon contaminations, while the loss of sensitivity is minimal [5, 9].

- $E_i^{hem} - E_i^{id} < 12.0$ GeV, for all the π and ρ hemispheres. These cuts reduce the ρ, π and $\pi\pi^0\pi^0$ misidentification, since they require almost all the energy, for both neutral and charged energies, to be identified. E_i^{hem} is the neutral plus charged energy of the ith hemisphere.

- $|\cos\theta_1| < 0.85$. This cut reduces the misidentification due to missing particles close to the beam axis. The sensitivity to transverse spin correlations goes as $\sin^2\theta_1$ and therefore the rejected events give a very small contribution.

6

An additional cut is applied to increase the sensitivity to the transverse spin correlations. The momentum of the identified particle should be greater than 4.0 GeV/c. This cut removes a momentum interval where the function $Q_3^{ij}(\epsilon)$ has a sign opposite to the average for particles with momentum greater than 4.0 GeV/c, and, consequently, it increases the sensitivity as a function of the acollinearity.

Class	e/μ	π	ρ	$\pi\pi^0\pi^0$	$n\pi/K$
e/μ	0.9947 ± 0.0004	0.0039 ± 0.0003	0.0011 ± 0.0002	0.0001 ± 0.0001	0.0001 ± 0.0001
π	0.0152 ± 0.0009	0.9061 ± 0.0020	0.0573 ± 0.0019	0.0191 ± 0.0010	0.0022 ± 0.0003
ρ	0.0003 ± 0.0001	0.0027 ± 0.0003	0.9302 ± 0.0015	0.0591 ± 0.0013	0.0078 ± 0.0005

Table 1: Fraction of events generated in class "i" and identified in class "j", M_i^j. The generated classes are given in the first row, and the reconstructed classes in the first column.

The channel mixing due to decay mode misidentification is calculated with a full detector Monte Carlo simulation. The mixing matrix is defined such that the $i-j$ element (M_i^j) is defined as the fraction of events classified as belonging to the "i" channel which is generated in the "j" channel. To include any possible bias from the cuts and detector effects the matrix is computed after the $\tau^+\tau^-$ event selection described above. The matrix is shown in Table 1, where only the statistical errors are included.

The number of events selected in each class is shown in Table 2.

Channel	$e^\pm\mu^\mp$	$l^\pm\pi^\mp$	$l^\pm\rho^\mp$	$\pi^\pm\pi^\mp$	$\pi^\pm\rho^\mp$	$\rho^\pm\rho^\mp$
Data	2853	4306	6367	820	2336	1677
e^+e^-	0	5.7 ± 2.0	6.4 ± 2.1	0	0	0
$\mu^+\mu^-$	0.52 ± 0.36	5.7 ± 1.2	1.0 ± 0.5	0.26 ± 0.26	0	0
total	0.52 ± 0.36	11.4 ± 2.3	7.4 ± 2.2	0.26 ± 0.26	0	0

Table 2: Number of real events selected in each channel, and non-τ contamination events estimated with the Monte Carlo.

3.3   Non-tau background

After all the cuts described above the background contamination in the sample is at the level of 10^{-3}. The contribution from Bhabha and dimuon events comes mainly from the misidentification of one electron or muon as a π or ρ. The contamination from $\gamma\gamma$ and $q\bar{q}$ events is negligible. The background estimation of Bhabha and dimuon events is based on Monte Carlo and is displayed in Table 2. The non-τ background is small, and therefore no correction is applied, but a systematic error is quoted instead.
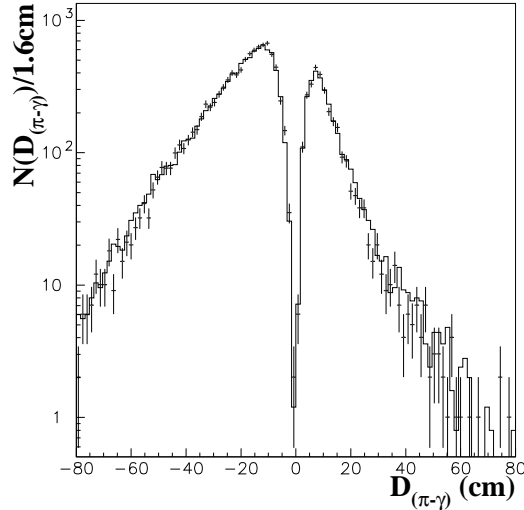
Figure 2: Minimum signed distance between a γ and the $\pi^{\pm}$ track extrapolation into ECAL for $\tau \to \rho$ decays. The data (points with error bars) and the MC prediction (solid histogram) normalized to the number of data entries agree over the entire spectrum.

3.4   Bias correction in the ρ channel

The decay of the ρ meson into $\pi^{\pm}\pi^0$ produces an angular asymmetry in the ρ identification. The ρ identification efficiency is reduced when a $\pi^{\pm}$ overlaps with a γ shower from a π^0 decay. The magnetic field bends the charged pion, breaking the azimuthal symmetry of its production with respect to the π^0 when it enters in ECAL. The signed distance [2] in ECAL between the γ's and the charged track computed for the data sample and Monte Carlo is shown in Fig. 2. The asymmetry in the ρ's is well described by the Monte Carlo.

The $\tau^+\tau^-$ Monte Carlo does not include transverse spin correlations and a fit to Monte Carlo generated events should therefore give a zero value for the C_{TT} and C_{TN} correlations. The values obtained from the fit to the Monte Carlo channels is taken as a bias on C_{TT} and C_{TN} due to this effect. These values are subtracted from those obtained when fitting the real data, and the statistical errors in the Monte Carlo fit are propagated accordingly, and included as a systematic error. The effect of the bias correction in the ρ reconstruction will be discussed in section 4.

4   Systematic errors

The values of the transverse spin correlation obtained from the likelihood fit are $C_{\mathrm{TT}} = 1.09 \pm 0.13$ and $C_{\mathrm{TN}} = 0.01 \pm 0.13$.

---

[2]The sign is computed depending on the position of the photon shower with respect to the track bending in the plane transverse to the beam axis.

Systematic errors coming from the Monte Carlo statistics are included in the statistical errors of the mixing matrix elements. To compute the resulting systematic errors on the transverse spin correlations C_{TT} and C_{TN}, the matrix elements are varied by $\pm 1\sigma$. This does not significantly affects the central value of C_{TT} and C_{TN} but the statistical errors do change. These new statistical errors are interpreted as the quadratic sum of the original statistical errors and the systematic errors, always considering the least favourable case. The same method is used to compute the systematic errors coming from the sources described in the following:

- Smearing of the polar and azimuthal angles. The angular smearing is computed from the difference between the reconstructed and the generated Monte Carlo angles. The likelihood fit is performed again convoluting the cross-section with the smearing of these angles.

- Errors on $\tau^{\pm}$ branching ratios [17]. The Monte Carlo is normalized to the world average τ branching ratios. These are then varied by $\pm 1\sigma$.

- Errors on the input parameters of the cross-section [17]: $\sin^2 \theta_{\mathrm{W}}^{\mathrm{eff}} = 0.2315 \pm 0.0004$, $M_Z = 91.1884 \pm 0.0022$, and $\Gamma_Z = 2.4963 \pm 0.0032$. The resulting systematic errors are negligible.

The correction due to the ρ reconstruction asymmetry is determined from the fit to the Monte Carlo events. The fit yields $C_{TT} = -0.03 \pm 0.04$ and $C_{TN} = 0.07 \pm 0.04$. The central value is taken as a bias and the statistical error from the fit is taken as systematic uncertainty. A possible uncertainty in the simulation of the effect is considered to be negligible compared to the fit errors since the data and Monte Carlo are in excellent agreement (see Fig. 2).

As mentioned in section 3.3, the non-τ background contribution is included as a systematic error in the measurement of C_{TT} and C_{TN}. The Monte Carlo provides a sample of background events passing the selection cuts. The likelihood function is then maximized subtracting the likelihood contributions of these events. This is equivalent to subtracting from the data sample the events corresponding to the predicted background. The systematic errors are then taken as the difference between the mean value of the transverse spin correlations with and without the non-τ background.

The systematic errors from initial state radiation (ISR) are split into two contributions:

- The assumption that the ISR is collinear with the beam direction. The systematic errors are estimated as the difference between the values obtained with the cosine of the angle of the ISR photons fixed to 1 and 0.95 (corresponding to the minimum angle of detected ISR photons). This is clearly an upper limit on the errors, which is nevertheless negligible.

- The variation of $Q_i(\epsilon)$ with the centre of mass energy after radiation. The systematic errors are computed varying the maximum value of x from 0.2 to approximately 1.

9

In principle, the transverse spin correlations are independent of a weak dipole form factor, $\tilde{d}_\tau$. However, the transverse spin polarization $\tilde{d}_\tau(s^T_{\tau-} - s^T_{\tau+})\sin\theta\cos\theta$ contributes to the term in the cross-section $\sin^2\theta_1\sin(2\phi)$, from which the C_{TN} spin correlation is derived (Eq. (5) and (6)). The limit already published by the ALEPH collaboration [7] is used to estimate the uncertainty induced in C_{TN}.

The contributions to the final systematic errors are shown in Table 3.

Source	ΔC_{TT}	ΔC_{TN}
Mixing	0.014	0.014
Angle smearing	0.003	0.003
Non-τ background	0.020	0.007
ISR	0.002	0.001
ρ asymmetry correction	0.039	0.040
τ decay branching ratios	0.009	0.009
$\tilde{d}_\tau$ residual contribution	- - -	0.002
Total	0.05	0.04

Table 3: Systematic uncertainties on the fitted transverse spin correlations.

5 Results

The values of the transverse spin correlations, with the bias correction applied are:

$$
\begin{aligned}
C_{\text{TT}} &= 1.06 \pm 0.13(stat) \pm 0.05(syst)\\
C_{\text{TN}} &= 0.08 \pm 0.13(stat) \pm 0.04(syst),
\end{aligned}
$$

in agreement with the Standard Model prediction.

The value of the C_{TT} transverse spin correlation clearly indicates that the axial vector coupling of the $Z\tau\tau$ vertex is larger than the vector coupling. The measured value is $\approx 15\sigma$ away from -1, i.e., pure vector coupling. Fig. 3 displays the allowed region in the (v_τ, a_τ) plane (shaded area).

The values of the longitudinal polarization and the transverse-normal spin correlation can be combined to obtain the phase difference between the axial vector and vector coupling as described in section 2.1. From the world average value of the longitudinal τ polarization [18]:

$$
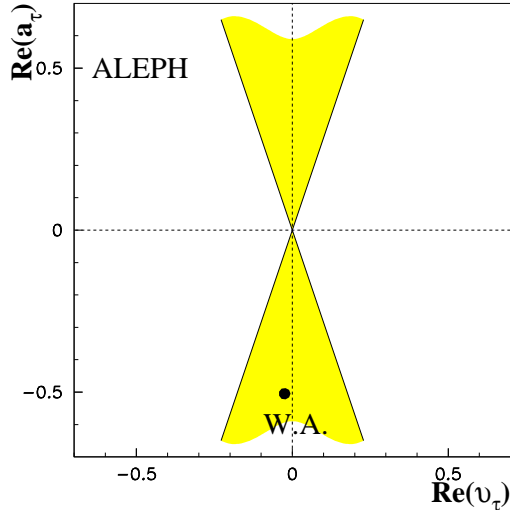P_\tau = -0.140 \pm 0.007, \tag{11}
$$

Figure 3: 95% C.L. allowed region (shaded) for the $\text{Re}(v_\tau)$ and $\text{Re}(a_\tau)$ couplings. The black point shows the world averaged (W.A.) values for the v_τ and a_τ couplings.

and the C_{TN} value reported here, the phase difference between the vector and axial vector couplings is

$$\tan(\Phi_{v_\tau} - \Phi_{a_\tau}) \;\; = \text{-0.57} \; \pm \; 0.97, \tag{12}$$

which is consistent with 0.07 predicted in the Standard Model.

The transverse spin correlations have also been calculated for each τ decay mode independently as shown in Table 4. The results are consistent.

The aplanarity dependence of the different channels is compared with the predictions of the Standard Model, $C_{\text{TT}} = 0.99$ and $C_{\text{TN}} = -0.01$, in Fig. 4. The predicted $\cos 2\phi$ dependence is clearly visible. Evidence for the C_{TT} spin correlation has been previously presented by the DELPHI collaboration using the same aplanarity observable [19].

6 Summary

A measurement of the transverse spin correlations in $\tau^+\tau^-$ production at the Z has been presented. The measured values,

$$C_{\text{TT}} = 1.06 \; \pm \; 0.14$$

and

$$C_{\text{TN}} = 0.08 \; \pm \; 0.14,$$

are consistent with the Standard Model predictions, $C_{\text{TT}} = 0.99$ and $C_{\text{TN}} = -0.01$. In particular, from the measurement of C_{TT} alone, it follows that $|a_\tau| \gg |v_\tau|$. Within the precision of the measurement the imaginary part of the $a_\tau^* v_\tau$ is consistent with zero.
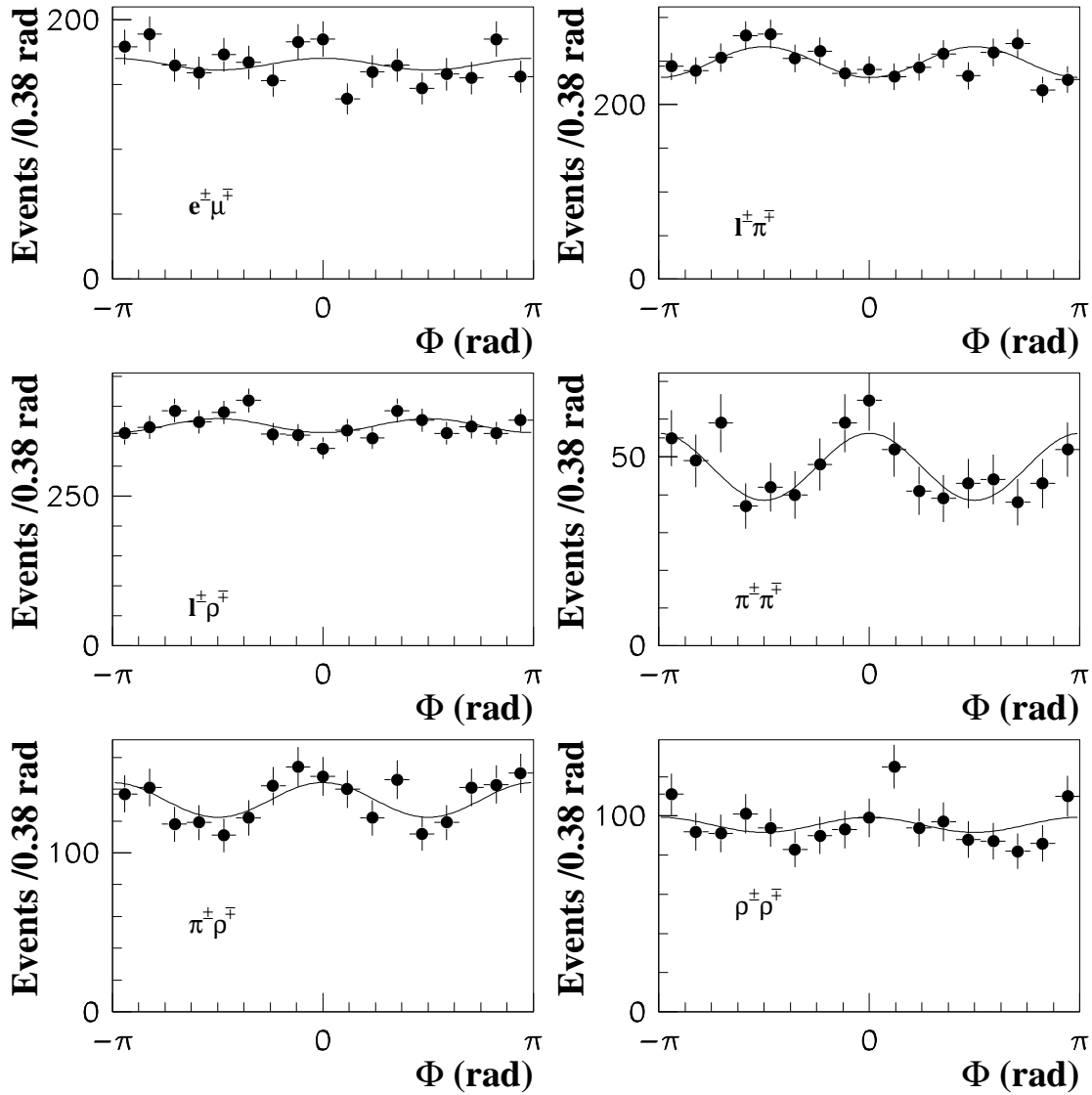
11

ALEPH

Figure 4: Number of events versus the aplanarity angle, ϕ (solid points). The curve shows the Standard Model prediction normalized to the total number of events.

Decay mode	C_{TT}	C_{TN}	
$e^{\pm}\mu^{\mp}$	$0.92\ \pm\ 0.70$	$-0.92\ \pm\ 0.71$	3.2%
$l^{\pm}\pi^{\mp}$	$0.79\ \pm\ 0.24$	$-0.01\ \pm\ 0.24$	27.1%
$l^{\pm}\rho^{\mp}$	$1.25\ \pm\ 0.50$	$0.12\ \pm\ 0.51$	4.6%
$\pi^{+}\pi^{-}$	$1.03\ \pm\ 0.19$	$0.07\ \pm\ 0.20$	41.7%
$\pi^{\pm}\rho^{\mp}$	$1.36\ \pm\ 0.32$	$0.38\ \pm\ 0.32$	20.8%
$\rho^{+}\rho^{-}$	$2.08\ \pm\ 0.71$	$0.68\ \pm\ 0.75$	2.65%
Total	1.06 ± 0.13	0.08 ± 0.13	
	$\chi^2 = 4.4\ \ C.L. = 49.3\%$	$\chi^2 = 3.6\ \ C.L. = 65.4\%$	

Table 4: Transverse spin correlation for the various decay modes. The last column shows the contribution of each channel to the averages.

Acknowledgements

It is a pleasure to thank to our colleagues in the accelerator divisions of CERN for the excellent performance of the LEP accelerator. Thanks are also due to the technical personnel of the collaborating institutions for their support in constructing and maintaining the ALEPH experiment. Those of us not from member states wish to thank CERN for its hospitality.

References

[1] ALEPH Collaboration, Phys. Lett. B265 (1991) 430.
    ALEPH Collaboration, Z. Phys. C69 (1996) 183.

[2] OPAL Collaboration, Phys. Lett. B266 (1991) 201.
    OPAL Collaboration, Z. Phys. C65 (1995) 1.
    OPAL Collaboration, CERN-PPE/96-078.

[3] L3 Collaboration, Phys. Lett. B294 (1992) 466.
    L3 Collaboration, Phys. Lett. B341 (1994) 245.

[4] DELPHI Collaboration, Z. Phys. C55 (1992) 555.
    DELPHI Collaboration, Z. Phys. C67 (1995) 83.

[5] J. Bernabéu, N. Rius and A. Pich, Phys. Lett. B257 (1991) 219.

[6] U. Stiegler, Z. Phys. **C58** (1993) 601.

[7] ALEPH Collaboration, Phys. Lett. B297 (1992) 459,
    ALEPH Collaboration, Phys. Lett. B346 (1995) 371,
    ALEPH Collaboration, Contribution to Warsaw conference, PA08-030 (1996),
    OPAL Collaboration, Phys. Lett. B281 (1992) 405,
    OPAL Collaboration, Z. Phys. C66 (1995) 31.

[8] J. Bernabéu and N. Rius, Phys. Lett. B232 (1989) 127.

[9] F. Sánchez, Phys. Lett. B384 (1996) 277.

[10] S. Jadach, J.H. Kuhn and Z. Wąs, Comput. Phys. Commun. 64 (1991) 275.

[11] F. Sánchez and Z. Wąs, Phys. Lett. B351 (1995) 562.

[12] W. Hollik, "Predictions for e^+e^- Processes", MPI-Ph/93-22, BI-TP 93/33;
R. Miquel, "Radiative Corrections to the Process $e^+e^- \rightarrow \nu\nu\gamma$", Ph.D. thesis,
Universitat Autónoma de Barcelona, unpublished (1989).

[13] ALEPH Collaboration, Nucl. Inst. and Meth. A294 (1990) 121.

[14] ALEPH Collaboration, Nucl. Inst. and Meth. A360 (1995) 481.

[15] ALEPH Collaboration, Z. Phys. C70 (1996) 561.

[16] ALEPH Collaboration, Z. Phys. C70 (1996) 579.

[17] Particle Data Group, R.M. Barnett et al., Phys. Rev. D54 (1996), 1.

[18] The LEP Collaborations ALEPH, DELPHI, L3, OPAL and the LEP Electroweak
Working Group, "A Combination of Preliminary Electroweak Measurements and
Constraints on the Standard Model", CERN-PPE/96-183.

[19] "First Evidence of transverse spin correlations in Z^0 Decays", Contribution to
HEP conference, EPS-HEP 95 Ref. EPS0765, DELPHI 95-111 PHYS 546.